Int. J. Heat Mass Transfer. Vol. 36, No. 17, pp. 4275–4281, 1993
Printed in Great Britain

0017–9310/93 $6.00 + 0.00

Numerical solution of natural convective heat transfer in parabolic enclosures

S. O. TALABI and U. NWABUKO
Mechanical Engineering Department, University of Lagos, Lagos, Nigeria

(*Received* 22 *September* 1992)

Abstract—Laminar free convective heat transfer within parabolic enclosures has been investigated using numerical computation methods. The geometry is a long cavity made up of a parabolic wall bowed over a horizontal wall. Due to symmetry, the analytical model is one-half of a two-dimensional cross-section consisting of a hot parabolic upper-wall, a cold horizontal base and an adiabatic vertical wall. Two cases of heat input from the parabolic upper-wall have been considered, namely (i) isothermal condition on the hot wall, and (ii) constant heat-flux through the hot wall. The base and vertical walls are made isothermal and adiabatic, respectively. A finite difference technique called 'staggered differencing' (SD) for both regular and irregular boundaries is applied in the iterative solution of the mass, momentum and energy equations. Steady state solutions have been obtained for the heat transfer to the cold base in the form of local and mean Nusselt numbers for $0.05 \leqslant H/B \leqslant 1.0$, $0 \leqslant Gr_B \leqslant 10^9$, $0.73 \leqslant Pr \leqslant 20$ and $0 < C_{ft} \leqslant 0.33$. Results show that in case (i) the heat transfer rate to the cold wall increases with increase in Gr and Pr but decreases with increase in H/B and C_{ft}, except for an anomaly for $C_{ft} = 0.33$, i.e. the circular profile. In case (ii), the heat transfer rate increases with increase in Gr, H/B, Pr and C_{ft}.

INTRODUCTION

STUDIES of laminar free convection in parabolic enclosures may be readily appreciated in consideration of the following two applications: (i) roofing-design of buildings for efficient air conditioning and (ii) design of efficient solar stills.

With respect to the former, roofing-designs are usually based on gross empirical formulations that are more suited to flat-top roofing than the more common pitched top, or the less common curved-top. Fundamental theoretical investigations that would really explain the intricate heat-transfer phenomena in the various roofings are often bypassed. Recently, however, there has been quite a few research studies akin to the heat transfer phenomena in flat-roofs as modelled by rectangular cavities, and to pitched-roofs as modelled by triangular cavities. Free convective heat transfer in rectangular cavities include the works of Poots [1], Davis [2], Newell and Schmidt [3], MacGregor and Emery [4], Elder [5] and Yin *et al.* [6]. Studies on triangular cavities include those of Akinsete and Coleman [7] and Flack and Witt [8]. These studies, some of which have been both theoretical and experimental, have enhanced the scientific knowledge of the heat transfer processes in the triangular and rectangular roofing types. Nevertheless, quite a few buildings have curved (parabolic) tops. These are often found in green houses, industrial buildings, arenas, nuclear power plants and houses in extreme-temperature regions of the world.

With respect to the second area of application, i.e. solar stills, most are designed in the form of plain glass or plexiglas placed horizontally or inclined over sets of heat absorbers, as elaborated by Edwards [9]. A clock-work mechanism is sometimes incorporated to rotate the collectors as the sun moves across the sky. However, a curved (convex) surface not only collects sun-rays from over a much wider range, but also concentrates the rays better than does a plain surface. A parabolic-surface collector, therefore, could operate effectively without a tilting mechanism, once it is properly installed.

Analytic studies of natural convection within concentric cylinders and spheres include the works of Powe *et al.* [10], Mack and Bishop [11], Mack and Hardee [12], Carley *et al.* [13] and Hodonett [14] while experimental studies include those of Scanlan *et al.* [15], Weber *et al.* [16] and Pneuli [17].

The present research is thus primarily aimed at the following two objectives: (i) to determine the free convective heat transfer characteristics for regions within curved roof-tops, and (ii) to find possible optimum surface curvatures for the design of solar collectors.

MATHEMATICAL FORMULATION

Analytical model

The analytical model consists of a two-dimensional cross-section of a roof which is infinite along its axis (Fig. 1(a)). Due to symmetry, the half-problem is used in the analytical formulation as a domain bounded above by a parabolic hot wall, HB, a horizontal cold wall, OB and an adiabatic wall, OH (Fig. 1(b)).

Governing equations

The fluid within the cavity is assumed to be inviscid, incompressible, Newtonian with constant properties.

NOMENCLATURE

A	area of parabolic enclosure
b	variation parameter of parabola (Fig. 1(b))
B	characteristic length = model base length [m]
C_{ft}	concavity factor = ratio of area HBS to area HBO (Fig. 1(b))
C_p	specific heat capacity at constant pressure [J kg^{-1} K^{-1}]
g	gravitational acceleration [m s^{-2}]
Gr	Grashof number, $(g\beta\Delta TB^3/\nu^2)$
h	heat transfer coefficient [W m^{-2} K^{-1}]
H	height of parabolic enclosure [m]
i	generalised node point
k	coefficient of thermal conductivity [W m^{-1} K^{-1}]
M	total number of nodes in a grid system
Nu_x	local Nusselt number, hx/k
Pr	Prandtl number, $\nu/\alpha = \mu C_p/k$
q	heat flux [W m^{-2}]
T	temperature [°C]
u	x-component of velocity [m s^{-1}]
U	dimensionless velocity in x-direction
U^*	characteristic velocity scale, $\nu Gr^{1/2}/B$
v	y-component of velocity [m s^{-1}]
V	dimensionless velocity in y-direction.

Greek symbols

α	coefficient of thermal diffusivity [m^2 s^{-1}]
β	coefficient of volume expansion [°C^{-1}]
θ	dimensionless temperature, $(T-T_c)/(T_H-T_c)$ or $(T-T_c)/(q_nB/k)$
μ	dynamic viscosity [N s m^{-2}]
ν	kinematic viscosity [m^2 s^{-1}]
ϕ	general function for field variables
ψ	stream function [m^2 s^{-1}]
Ψ	dimensionless stream function
ω	vorticity [s^{-1}]
Ω	dimensionless vorticity.

Subscripts

c	cold wall
B	based on characteristic length, B
H	hot wall
n	normal direction
w	wall condition
x	local value at x.

The flow field is two-dimensional with negligible viscous dissipation. Introducing the dimensional characteristic variables such that

$$X = \frac{x}{B}, \quad Y = \frac{y}{B}, \quad U = \frac{u}{U^*}, \quad V = \frac{v}{U^*},$$

$$\theta = \frac{T-T_c}{T_H-T_c} \quad \text{or} \quad \frac{T-T_c}{q_nB/k}$$

$$\Psi = \frac{\psi}{U^*B} \quad \text{and} \quad \Omega = \frac{\omega B}{U^*}$$

in the conservation equations, there results the following dimensionless equations:

$$\frac{\partial^2\Omega}{\partial X^2} + \frac{\partial^2\Omega}{\partial Y^2} - Gr^{1/2}\left(U\frac{\partial\Omega}{\partial X} + V\frac{\partial\Omega}{\partial Y}\right) - Gr^{1/2}\frac{\partial\theta}{\partial X} = 0 \quad (1)$$

$$\frac{\partial^2\theta}{\partial X^2} + \frac{\partial^2\theta}{\partial Y^2} - Pr\,Gr^{1/2}\left(U\frac{\partial\theta}{\partial X} + V\frac{\partial\theta}{\partial Y}\right) = 0 \quad (2)$$

where

$$U = \frac{\partial\Psi}{\partial Y} \quad (3)$$

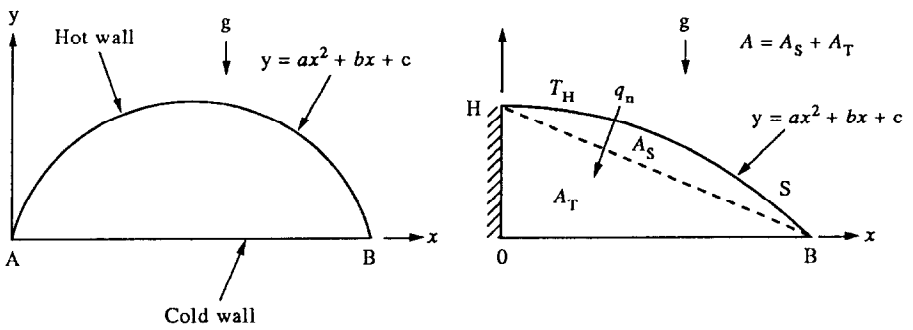

(a) The full problem (a) The half problem

FIG. 1. Analytical models of the physical problem.

$$V = -\frac{\partial \Psi}{\partial X} \tag{4}$$

and

$$\frac{\partial^2 \Psi}{\partial X^2} + \frac{\partial^2 \Psi}{\partial Y^2} + \Omega = 0. \tag{5}$$

Equation (1) is obtained from the X- and Y-components of the momentum equation after eliminating the pressure terms by cross-differentiation. The above set of equations is subject to the following boundary conditions:

$$U = V = 0, \quad \text{at all walls} \tag{6a}$$

$$\Psi = 0, \quad \text{at all walls} \tag{6b}$$

$$\theta = 0, \quad \text{at the cold wall} \tag{7a}$$

$$\frac{\partial \theta}{\partial X} = 0, \quad \text{at the adiabatic wall} \tag{7b}$$

$$\theta = 1, \quad \text{at the hot wall (Case I)} \tag{8a}$$

$$\frac{\partial \theta}{\partial n} = -1, \quad \text{at the hot wall (Case II)} \tag{8b}$$

$$\frac{\partial V}{\partial x} - \frac{\partial U}{\partial Y} = \Omega \quad \text{at all walls} \tag{9}$$

where n is the direction normal to the curved hot surface.

Geometric parameters

The theoretical analysis considers a generalised parabolic profile. However, the numerical computations require some parameters to characterise the physical variations of the enclosure. For this purpose, the height-to-base ratio, H/B characterises the size of the domain while the concavity factors, C_{ft} characterise the profile, i.e. the size of bulge (Fig. 1(b)).

Irregular boundaries

The parabolic hot wall creates the problem of irregular boundary in the application of the finite difference numerical solution technique. This makes it very difficult to deal with the Neuman-type of boundary condition. Moreover, high Grashof number range of solutions require large number-of-nodes in the discretisation process. The resultant effect is that the application of special routines as prescribed by Smith [18] and Carnahan *et al.* [19] for the computation of derivatives at normalised boundary nodes becomes rather tedious.

This problem is overcome by normalising all the irregular boundary nodes and applying the staggered differencing (SD) computational technique due to Nwabuko [20].

When the differential equations for the field variables (equations (1)–(3)) are cast into the SD form, they acquire the following general format:

$$\sum_{j=0}^{4} A_{ij}\Phi_j = D_i, \quad i = 1, 2, \ldots, M$$

i.e.

$$A_{i0}\Phi_0 + A_{i1}\Phi_1 + A_{i2}\Phi_2 + A_{i3}\Phi_3 + A_{i4}\Phi_4 = D_i \qquad i = 1, 2, \ldots, M \tag{10}$$

where, Φ is a general function representing a field variable such as θ, Ψ and Ω. The coefficients of Φ, i.e. the A_{ij}s, depend on the particular variable being considered where, at a given point, $i = j = 0$ when the referenced local node corresponds to the global node under computation (Fig. 2). For example, when the energy equation (2) is considered, the coefficients of θ are given as

$$\left.\begin{aligned} A_{i0} &= (\gamma_0 + \delta_0 - \alpha_0 Pr\, GU_i - \beta_0 Pr\, GV_i) \\ A_{i1} &= (\gamma_1 + \alpha_1 Pr\, GU_i) \\ A_{i2} &= (\delta_2 + \beta_2 Pr\, GV_i) \\ A_{i3} &= (\gamma_3 + \alpha_3 Pr\, GU_i) \\ A_{i4} &= (\delta_4 + \beta_4 Pr\, GV_i) \\ D &= 0 \end{aligned}\right\} \tag{11}$$

where $G = Gr^{1/2}$, α, β, γ and δ are functions of the local ΔX and ΔY relative to the node point i and Pr is Prandtl number.

Solution procedure

The numerical solution procedure consists of cyclic Gauss–Seidel iterative computation on the set of SD representations of the governing equations (1)–(5), while imposing the respective boundary conditions for each equation in turn. The sequence is as follows:

(i) A specification of H/B and C_{ft}, the geometric parameters, initialises the automatic mesh-generator which constructs and stores an appropriate solution grid.

(ii) The main program picks up the energy equation (2) in the form of equation (10), imposes the set of temperature boundary condition equations ((7a), (7b) and (8a)) or ((7a), (7b) and (8b)), depending on whether Case I or Case II is specified. Then with an arbitrary initial temperature distribution (usually zero) within the domain and zero velocity at all the nodes, the energy equation is solved iteratively to convergence. This would be the pure conduction solution corresponding to $Gr = 0$.

(iii) When a Grashof number, $Gr > 0$ is specified,

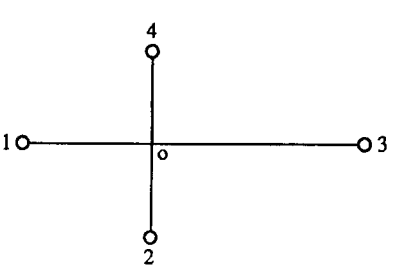

FIG. 2. Local node identification.

the wall velocities are retained as zero and the energy equation is solved in full as

$$\theta_i^{(k+1)} = \frac{1}{A_{i0}}(-A_{i1}\theta_{i1}^{(k)} - A_{i2}\theta_{i2}^{(k)} - A_{i3}\theta_{i3}^{(k)} - A_{i4}\theta_{i4}^{(k)}) \tag{12}$$

using the convergence criterion,

$$|\theta_i^{k+1} - \theta_i^k| \leqslant 10^{-4}.$$

The converged temperature values $\theta_{i-1,M}^{k+1}$ are stored separately as $\theta_{i-1,M}^{n}$, for later use in tests for global convergence.

(iv) The vorticity equation (1) is solved next. It requires wall vorticity Ω_w for its solution. This is provided by using the latest computed values of U and V along the walls in equations (3) and (4) to obtain Ψ_i which is then used in equation (5) to obtain Ω_w along the walls. After this, the interior values of Ω_i are solved for iteratively, with the SD representation of equation (1), until convergence is obtained.

(v) The stream function equation is then solved. Boundary conditions are specified as $\Psi = 0$ on all walls. Arbitrary initial distribution of $\Psi = 0$ is effected on the interior and the SD representation of equation (5) is solved iteratively until convergence is obtained for Ψ.

(vi) The latest values of Ψ are used in equations (3) and (4) for direct computation of U- and V-velocity components, respectively.

(vii) Using current values of U and V, the computational procedure returns to step (iii) and the energy equation is solved once again. Local convergence of θ now produces $\theta_{i-1,M}^{n+1}$ which may then be compared with the previous $\theta_{i-1,M}^{n}$ to determine global convergence. If $\theta_{i-1,M}^{n+1}$ and $\theta_{i-1,M}^{n}$ meet the convergence criterion, a solution of the overall problem is deemed to have been achieved for the specified Gr, otherwise, the scheme moves down to step (iv), i.e. the solution of vorticity equation, after replacing $\theta_{i-1,M}^{n}$ with $\theta_{i-1,M}^{n+1}$.

(viii) Whenever global convergence is achieved the local and mean Nusselt numbers Nu_x and $\overline{Nu}_x$ are computed, respectively as

$$Nu_x = \left.\frac{\partial\theta}{\partial Y}\right|_{Y=0} \tag{13}$$

$$\overline{Nu}_x = \frac{1}{B}\int_0^B Nu_x \, \mathrm{d}x. \tag{14}$$

The integration in equation (14) is carried out by a numerical trapezoidal integration sub-program.

Higher Grashof numbers require finer discretisation which creates more nodes. Thus, three different half-mesh sizes of 15×15 (120 nodes), 29×29 (435 nodes) and 57×57 (1653 nodes) were used for a Grashof number range $0 \leqslant Gr \leqslant 10^9$, depending on the value of H/B.

RESULTS AND DISCUSSION

In the presentation of the distribution of the field variables and heat transfer characteristics, values of $H/B = 0.25$ and $C_{11} = 0.33$ (i.e. circular segment) have been used. This choice is influenced by the relative ease of fabrication for both experimental and full scale applications. Also high Grashof numbers in the range $10^6 \leqslant Gr \leqslant 10^9$ have been used in consideration of the

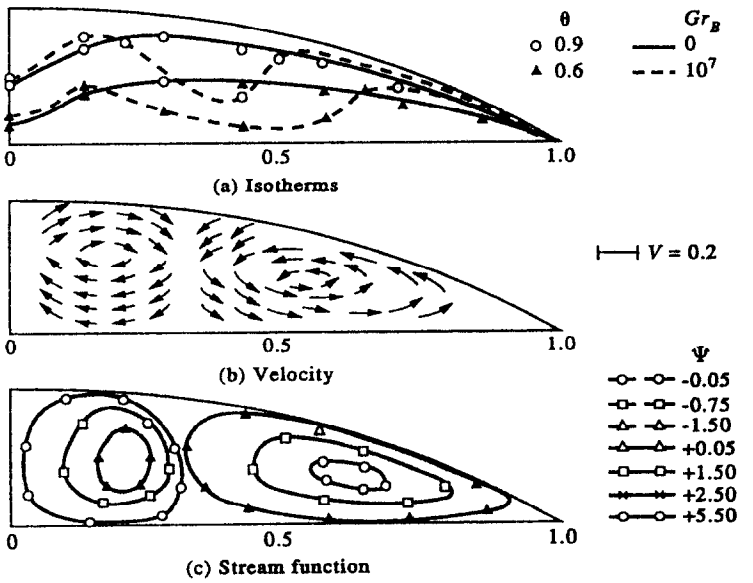

FIG. 3. Distribution of some field variables for the isothermal condition for $H/B = 0.25$, $C_{11} = 0.33$ and $Gr = 10^7$.

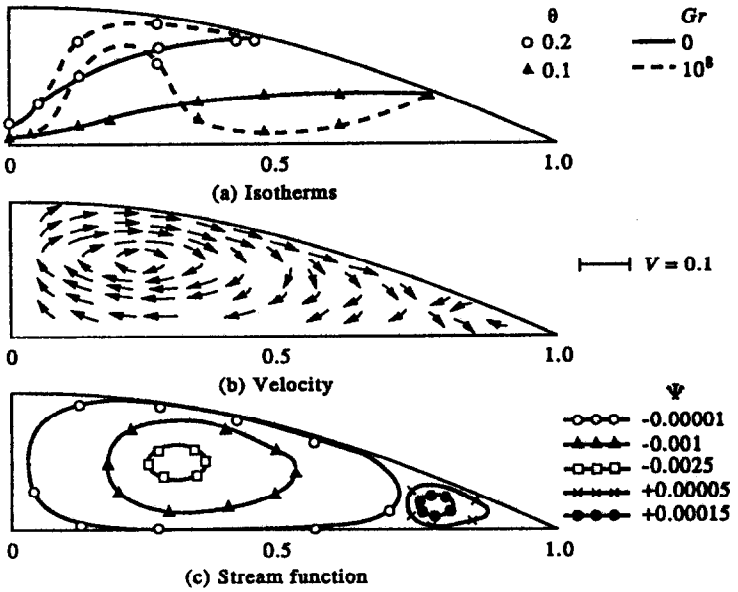

FIG. 4. Distribution of some field variables for the constant heat-flux condition for $H/B = 0.25$ and $C_{ft} = 0.33$ and $Gr = 10^8$.

practical applications discussed in the introduction. For example, it is estimated that an average solar heat flux of 1 kW m^{-2} reaches the earth's surface around noon each day and this translates to a Grashof number of about 10^9 for the constant heat flux case.

Figures 3(a)–(c) show the distribution of temperature, resultant velocity vector and stream function, respectively for $H/B = 0.25$, $C_{ft} = 0.33$ and $Gr = 10^7$. Of interest is the remarkable contrast between the $Gr = 0$ (pure conduction) and $Gr = 10^7$ patterns in Fig. 3(a). This pattern is consistent with the dual streamline pattern of Fig. 3(c). Figures 4(a)–(c) are the constant heat-flux (Case II) versions of Figs. 3(a)–(c). A double-flow pattern also exists in this case but the magnitudes and positions of the patterns differ.

Figure 5 shows the local Nusselt number, Nu_x dis-

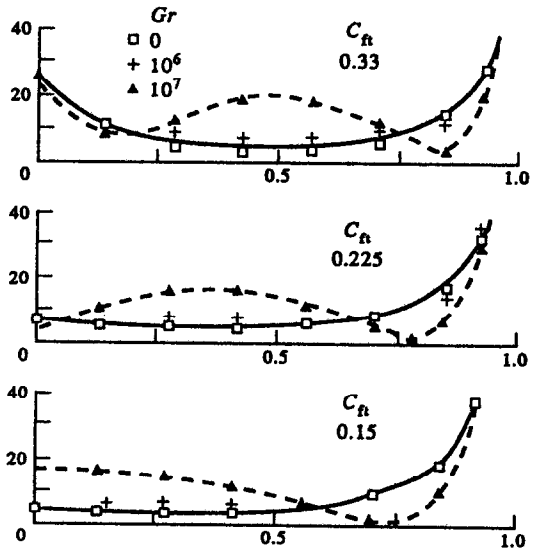

FIG. 5. Local Nusselt number, Nu_x distribution along cold wall for isothermal condition for $H/B = 0.25$.

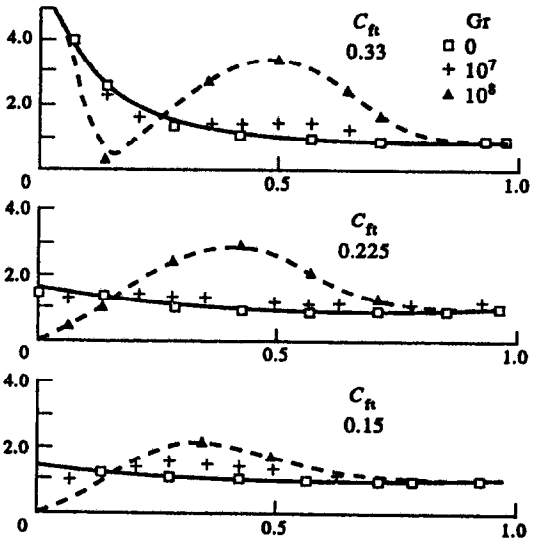

FIG. 6. Local Nusselt number, Nu_x distribution along the cold wall for the constant heat-flux condition for $H/B = 0.25$.

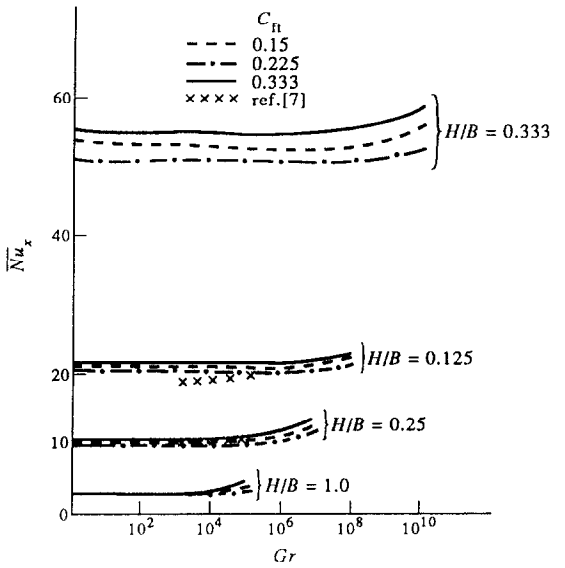

FIG. 7. Mean Nusselt number vs Grashof number for various concavity factors ($0.15 \leqslant C_{ft} \leqslant 0.33$) and ($0.05 \leqslant H/B \leqslant 1.0$) for isothermal hot-wall, Case I.

tribution along the cold wall for Case I, for $C_{ft} = 0.33$, 0.225 and 0.15, respectively. The local heat transfer rate is almost indistinguishable for $Gr = 0$ and $Gr = 10^6$. However, a distinctive heat transfer pattern emerges for $Gr = 10^7$. It is obvious from the patterns of Figs. 3 and 5 that the effects of convection currents become significant in the range $Gr \geqslant 10^7$. In the latter figure, one observes that a large fraction of the heat transfer is concentrated in the last one-third of the base. This condition is fairly consistent for all C_{ft}s considered. However, the fraction of the overall heat that is transferred through this $\frac{1}{3}$ length depends on the Gr range. A similar heat transfer pattern has been reported by Akinsete and Coleman [7] and Talabi [21] for triangular geometries.

Figure 6 is the constant heat-flux version of local Nusselt number distribution. It is easily observable that the last $\frac{1}{3}$ length does not have the concentrated heat-transfer of Case I but rather a relatively small value, mostly due to conduction.

Figures 7 and 8 are generalised plots of the mean Nusselt number as functions of Grashof number for Cases I and II, respectively, from which the general conclusions regarding heat transfer in parabolic enclosures can eventually be drawn. Some of the result data of ref. [7] have also been shown in Fig. 7 for $C_{ft} = 0$.

Finally, it would be instructive to compare the present results with some of those available for triangular enclosures and thus, draw some conclusion on their relative heat transfer characteristics.

(i) In the isothermal Case I, the heat transfer pat-

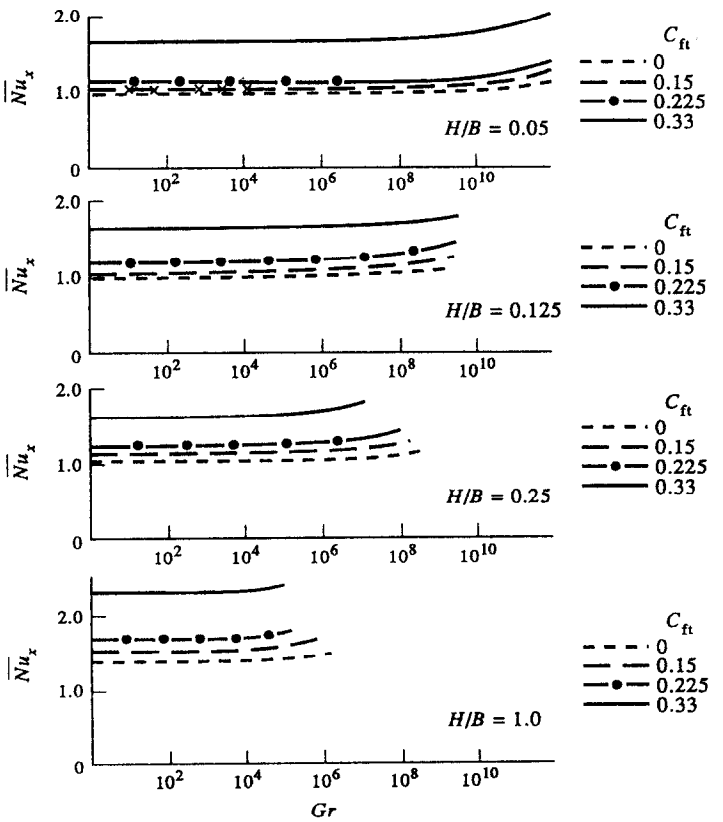

FIG. 8. Mean Nusselt number vs Grashof number for various concavity factors ($0 \leqslant C_{ft} \leqslant 0.33$) and ($0.05 \leqslant H/B \leqslant 1.0$) for constant heat-flux condition, Case II.

tern in the form of local Nusselt number Nu_x tends to be more uniformly distributed over the cold base for the parabolic section than the triangular section as reported by Akinsete and Coleman [7]. In the triangular case, the heat transfer rate is generally very high near the junction of the hot and cold walls. This pattern is similar to the ones obtained for the parabolic profiles at low Grashof number.

(ii) In the constant heat-flux Case II, the parabolic profile is seen to enhance convective heat transfer as may be observed from the higher overall heat-transfer rate along the cold wall in comparison to triangular profile. Besides, the local heat transfer rate is more uniform in Case II. In making the above two comparisons, the results of the most effective parabolic profile ($C_{ft} = 0.33$) which corresponds to a circular profile has been used. Nevertheless, the other parabolic profiles ($C_{ft} = 0.225$, 0.15, etc) show similar trends as those of $C_{ft} = 0.33$.

(iii) For the isothermal case, the heat transfer to the cold wall as measured by the mean Nusselt number, $\overline{Nu}_x$, increases slightly with increase in Gr and Pr (Fig. 7) but decreases with increasing H/B and increasing C_{ft}, with the exception of $C_{ft} = 0.33$, which can be considered an anomaly. This latter geometric configuration has the highest Nu_x next to $C_{ft} = 0.15$ instead of the expected lowest. This is consistent for all the H/B considered in Case I (Fig. 7).

(iv) For the constant heat-flux configuration, the heat transfer rate, $\overline{Nu}_x$, increases with increasing Gr, H/B, C_{ft} (Fig. 8) and Pr.

REFERENCES

1. G. Poots, Heat transfer by laminar free convection in enclosed plane gas layers, *Q. J. Mech. Appl. Math.* **11**, 257–273 (1958).
2. G. de Vahl Davis, Laminar natural convection in an enclosed rectangular cavity, *Int. J. Heat Mass Transfer* **11**, 1675–1693 (1968).
3. M. E. Newell and F. W. Schmidt, Heat transfer by laminar natural convection within rectangular enclosures, *J. Heat Transfer* **9**, 159–168 (1970).
4. R. K. MacGregor and A. F. Emergy, Free convection through vertical plane layers—moderate and high Prandtl number fluids, *J. Heat Transfer, Trans. ASME, Series C* **11**, 391–397 (1989).
5. J. W. Elder, Numerical experiments with free convection in a vertical slot, *J. Fluid Mech.* **24**, 823–843 (1965).
6. S. H. Yin, T. Y. Wung and K. Chen, Natural convection in an air layer enclosed within rectangular cavities, *Int. J. Heat Mass Transfer* **21**, 307–315 (1978).
7. V. A. Akinsete and T. A. Coleman, Heat transfer by steady laminar free convection in triangular enclosures, *Int. J. Heat Mass Transfer* **25**, 991–998 (1985).
8. R. O. Flack and G. L. Witt, Velocity measurements in two natural convection air flows using a laser velocimeter, *J. Heat Transfer, Trans. ASME, Series C* **101**, 256–200 (1979).
9. D. K. Edwards, *Solar Collector Design*. The Franklin Institute Press, Philadelphia, Pennsylvania (1977).
10. R. E. Powe, C. T. Carley and S. L. Carruth, A numerical solution for natural convection in cylindrical annuli, *J. Heat Transfer* **93c**(2), 210–220 (1971).
11. L. R. Mack and E. H. Bishop, Natural convection between horizontal concentric cylinders for low Rayleigh numbers, *Q. J. Mech. Appl. Math.* **21**, 223–241 (1968).
12. L. R. Mack and H. C. Hardee, Natural convection between concentric spheres at low Rayleigh numbers, *Int. J. Heat Mass Transfer* **11**, 387–396 (1968).
13. C. T. Carley, R. E. Powe and E. H. Bishop, Free convection flow patterns in cylindrical annuli, *J. Heat Transfer* **196**(3), 310–314 (1969).
14. P. F. Hodonett, Natural convection between horizontal heated concentric cylinders, *J. Appl. Math. Phys.* **24**, 507–516 (1973).
15. J. A. Scanlan, E. H. Bishop and R. E. Powe, Natural convection heat transfer between concentric spheres, *Int. J. Heat Mass Transfer* **13**, 1857–1872 (1970).
16. N. Weber, R. E. Powe, E. H. Bishop and J. Scanlan, Heat transfer by natural convection between vertically eccentric spheres, *J. Heat Transfer* **95c**(1), 47–52 (1973).
17. D. Pneuli, Upper and lower bounds to thermal instability criteria for completely confined fluids inside arbitrary configuration, *Int. J. Heat Mass Transfer* **18**, 1213–1218 (1975).
18. G. D. Smith, *Numerical Solution of Partial Differential Equations: Finite Difference Methods*. Clarendon Press, Oxford (1978).
19. P. Carnahan, H. A. Luther and J. O. Wilkes, *Applied Numerical Methods*. Wiley, New York (1969).
20. U. Nwabuko, Laminar free convective heat transfer in parabolic enclosures, Ph.D. Thesis, University of Lagos, Nigeria (1989).
21. S. O. Talabi, Numerical simulation of unsteady heat conduction in right-triangular domains: a second look, *Int. AMSE Conference on Modelling and Simulation*, Sorrento, Italy, Sept., 1986, Vol. 3.2, pp. 131–141 (1986).